

Learning Lattice Quantum Field Theories with Equivariant Continuous Flows

Mathis Gerdes,^{1,*} Pim de Haan,^{2,3,*} Corrado Rainone,³ Roberto Bondesan,³ and Miranda C. N. Cheng^{1,4,5}

¹*Institute of Physics, University of Amsterdam, the Netherlands*

²*QUVA Lab, University of Amsterdam*

³*Qualcomm AI Research, Qualcomm Technologies Netherlands B.V.[†]*

⁴*Korteweg-de Vries Institute for Mathematics, University of Amsterdam, the Netherlands*

⁵*Institute for Mathematics, Academia Sinica, Taipei, Taiwan*

We propose a novel machine learning method for sampling from the high-dimensional probability distributions of Lattice Quantum Field Theories. Instead of the deep architectures used so far for this task, our proposal is based on a single neural ODE layer and incorporates the full symmetries of the problem. We test our model on the ϕ^4 theory, showing that it systematically outperforms previously proposed flow-based methods in sampling efficiency, and the improvement is especially pronounced for larger lattices. Compared to the previous baseline model, we improve a key metric, the effective sample size, from 1% to 91% on a lattice of size 32×32 . We also demonstrate that our model can successfully learn a continuous family of theories at once, and the results of learning can be transferred to larger lattices. Such generalization capacities further accentuate the potential advantages of machine learning methods compared to traditional MCMC-based methods.

Introduction. Lattice field theory (LFT) remains the only robust and universal method to extract physical observables from a non-perturbative quantum field theory (QFT). As a result, the applications of such lattice computations are omnipresent in physics. Calculations for LFTs have traditionally relied on Markov Chain Monte Carlo (MCMC) methods. A well-known challenge these sampling methods face is the phenomenon of critical slowing down [1]. When moving towards the critical point or the continuum limit, consecutively generated samples become increasingly correlated as measured by a rapidly increasing *autocorrelation time* (time between statistically independent samples). In practice, this computational inefficiency constitutes a bottleneck for achieving high-accuracy results. While efficient algorithms exist for certain statistical mechanical models — e.g. the Swendsen-Wang algorithm for the Ising and Potts models [2] — a general approach is still lacking. An additional challenge arises from the fact that the entire sampling procedure typically needs to be initiated anew each time the theory is deformed, for instance by changing the UV cutoff (lattice spacing) or the coupling constants.

Rapid progress in machine learning provides new tools to tackle this complex sampling problem, see [3–20] for earlier related works. Flow-based models, in particular, offer a promising new framework for sampling which can mitigate the problem of critical slowing down and amortizes the costs of sampling by learning to approximate the target distribution. Moreover, since they estimate the likelihood of configurations they can be used to estimate some observables which are challenging to estimate with standard MCMC methods [21, 22]. In the flow

framework, a parametrized function f_θ is learned, which maps from an auxiliary “latent” space to the space of field configurations. It is optimized such that an easy-to-sample distribution ρ (e.g. an independent Gaussian) gets transformed, or pushed forward, to approximate the complex distribution given by the action of the theory [23]. The capability to incorporate physical symmetries of either the local or global type into the flow can moreover circumvent difficulties of sampling caused by the degeneracies of physical configurations which are related by symmetry actions [24].

The idea of applying a flow model to lattice field theory has been tested in [14] using the so-called real NVP model, and proof-of-concept experiments have been successfully carried out for small lattices. However, significant hurdles remain before a flow-based model can be applied in a physically interesting setup. For instance, it has been argued that these models require a training time that rises exponentially with the number of lattice sites [25]. In practice, it becomes infeasible to attain high ac-

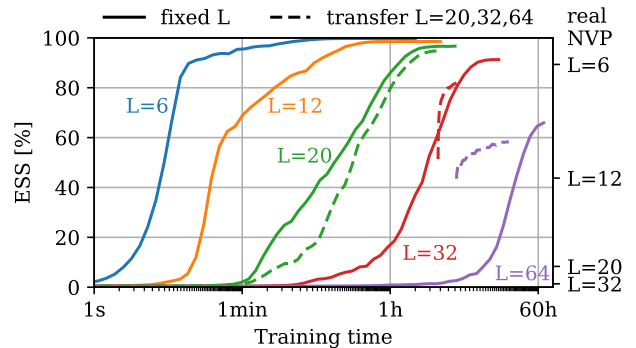


FIG. 1: The effective sample sizes for lattice sizes $L \times L$ of our model, compared to the real NVP baseline. Dashed lines show the learning trajectory of transfer learning from $L = 20$ to $L = 64$.

* Equal contribution

[†] Qualcomm AI Research is an initiative of Qualcomm Technologies, Inc.

ceptance rates on large lattices, while these are precisely the physically interesting regime.

To go beyond proof-of-concept studies, we devise a novel flow model¹ which improves the performance in the following three aspects, when compared to the state-of-the-art baseline model [14, 18, 25]: 1) scalability, 2) efficiency, and 3) symmetries. In more details, we contribute the following. 1) We propose a *continuous flow* model, where the inverse trivializing map f_θ is given as the solution to an ordinary differential equation (ODE). When applied to the two-dimensional ϕ^4 theory, our model dramatically improves a key metric, the effective sample size (ESS), to 91% at $L^2 = 32^2$ after about 10 hours of training as shown in Figure 1, in contrast with the 1.4% achieved by the real NVP model after approximately 2 weeks of training. Going further beyond what has been reported so far [25], we also obtain good results on lattices with $L^2 = 64^2$ vertices. Moreover, as opposed to the real NVP flow tested in [25], Figure 2 demonstrates that our continuous flow model is sample efficient in training and in particular does not display an exponentially growing training cost when lattice size increases. 2) We demonstrate the ability of our model to learn many theories at once in the following sense. First, we show that training efficiency can be gained by upscaling the network learned for lattice size L to a larger lattice of size L' . See Figure 1. Second, we train a family of flows $f_\theta^{(\psi)}$ parametrized by theory parameters ψ within a continuous domain, as used for Figure 3. Once the training is done, sampling is extremely cheap and no particular slowing down is encountered near the critical point. 3) In contrast to the real NVP architecture (cf. [26]), our model is equivariant to all symmetries of the LFT, including the full geometric symmetries of the lattice and the global symmetry of the scalar theory. If not built into the architecture, these symmetries are only approximately learned by the model, as exemplified in Figure 6 in the appendix.

Scalar Quantum Field Theory. Our goal is to improve the MCMC sampling performance for quantum field theories with scalar fields which possess non-trivial symmetry properties. We will now consider a scalar field theory on a two-dimensional periodic square lattice $V_L \cong (\mathbb{Z}/L\mathbb{Z})^2$. In particular, the *field configuration* is a real function $\phi : V_L \rightarrow \mathbb{R}$ on the vertex set V_L , and we denote by ϕ_x the value at the vertex $x \in V_L$. The theory is described by a probability density $p(\phi) = \exp(-S(\phi))/Z$ with action

$$S(\phi) = \sum_{x,y \in V_L} \phi_x \Delta_{xy} \phi_y + \sum_{x \in V_L} m^2 \phi_x^2 + \sum_{x \in V_L} V(\phi_x), \quad (1)$$

where $V : \mathbb{R} \rightarrow \mathbb{R}$ is a potential function, Δ is the Laplacian matrix of the periodic square lattice, and m^2 is a

numerical parameter. The partition function is defined as $Z = \int \prod_{x \in V_L} d\phi_x e^{-S(\phi)}$. For polynomials $V(\phi)$ of degree greater than two, the normalization factor Z and the moments of $p(\phi)$ are not known analytically, and are typically estimated numerically. The statistical correlations between spatially-separated degrees of freedom of the theory are measured by the *correlation length* ξ . As a result, it also controls the difficulty of directly sampling from $p(\phi)$.

We focus on the case where the potential is invariant to all spatial symmetries of the lattice and has a \mathbb{Z}_2 symmetry $V(\phi) = V(-\phi)$. This family of theories is also known as the Landau-Ginzburg model, and possesses a rich phase diagram with multi-critical points described by the unitary minimal model conformal field theories [28].

Samplers Based on Normalizing Flows. To correct for the approximate nature of the learned map, a Metropolis-Hastings step is applied to reject or accept the pushed-forward samples. This guarantees asymptotic exactness, while, assuming the *acceptance rate* is sufficiently high, the computational cost is not significantly increased. Recall that the Independent Metropolis-

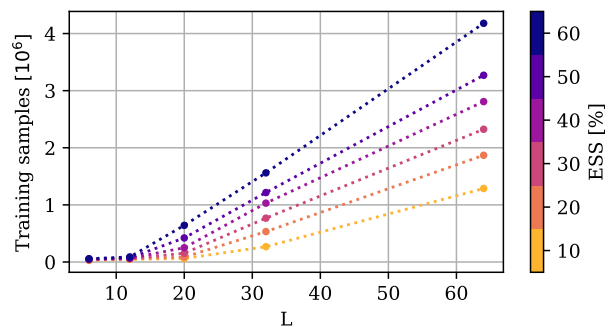


FIG. 2: Samples used during training until the values of ESS is attained, for lattice sizes $L = 6, 12, 20, 32, 64$.

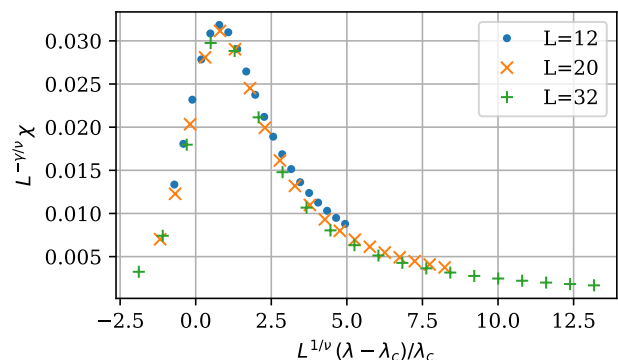


FIG. 3: Susceptibility estimated by MCMC chains of length 10^6 , rescaled using the Ising model critical exponents $\nu = 1$, $\gamma = 7/4$ to account for finite-size scaling. The used value $\lambda_c = 4.25$ of the critical coupling was chosen based on previous numerical results [27].

¹ An implementation can be found at <https://github.com/mathisgerdes/continuous-flow-lft>.

Hastings algorithm is a flexible method to sample from a target density p given a proposal distribution q [29]. At each time i , a proposed sample ϕ' drawn from the proposed distribution q is accepted with probability $\min(1, q(\phi^{(i-1)})p(\phi')/q(\phi')p(\phi^{(i-1)}))$, which depends on the previous sample $\phi^{(i-1)}$. Accepting the proposal means setting $\phi^{(i)} = \phi'$, else we repeat the previous value $\phi^{(i)} = \phi^{(i-1)}$. Traditionally, the distribution q is painstakingly handcrafted to maximize the acceptance rate. In contrast, the ML approach [30] to this problem is to learn a proposal distribution $q(\phi)$, for example by using a normalizing flow [14]. As mentioned before, in this framework $q(\phi)$ is given by the push-forward under a learned map f_θ of some simple distribution ρ such as a normal distribution. Since the proposals are generated independently, rejections in the ensuing Metropolis-Hastings step are the only source of autocorrelation.

When samples from p are available, q can be matched to p by optimizing the parameters θ to maximize the log-likelihood of those samples: $\mathbb{E}_{\phi \sim p}[\log q_\theta(\phi)]$. However, obtaining such samples requires expensive MCMC sampling which is precisely what we would like to avoid. Instead, we aim to minimize the reverse Kullback-Leibler (KL) divergence $\text{KL}(q|p)$, also known as the reverse relative entropy, which uses samples from the model distribution q :

$$\begin{aligned} \text{KL}(q|p) &= \mathbb{E}_{\phi \sim q}[\log \frac{q(\phi)}{p(\phi)}] \\ &= \mathbb{E}_{z \sim \rho}[\log q(f_\theta(z)) + S(f_\theta(z))] + \log Z. \end{aligned} \quad (2)$$

In the second equality, we have used the flow f_θ to replace samples from q by $f_\theta(z)$, where z denote samples of ρ . Note that the last term does not contribute to the gradient.

In our continuous normalizing flow model, we transform a sample $z \sim \rho$ with an invertible map $f_\theta : \mathbb{R}^{L^2} \rightarrow \mathbb{R}^{L^2}$, $z \mapsto \phi$, defined as the solution to a neural ODE [31] for time $t \in [0, T]$:

$$\frac{d\phi(t)_x}{dt} = g_\theta(\phi(t), t)_x \text{ with } z \equiv \phi(0), \phi \equiv \phi(T). \quad (3)$$

Here, the vector field $g_\theta(\phi(t), t)_x$ is a neural network with weights θ . The probability $q(\phi) \equiv p(\phi(T))$ of samples transformed by the flow, necessary for computing the KL divergence, can be obtained by solving another ODE [31] which contains the divergence of g_θ :

$$\frac{d \log p(\phi(t))}{dt} = -(\nabla_\phi \cdot g_\theta)(\phi(t), t) \quad (4)$$

with the boundary condition $p(\phi(0)) = \rho(z)$. For the network architectures of the vector field g_θ described below, the divergence can be computed analytically. The gradients of the KL divergence are computed with another ODE derived using the adjoint sensitivity method [31].

As mentioned in [32], if the vector field g_θ is equivariant to the symmetries of the theory and the chosen

latent space distribution is invariant under the symmetry action, then the resulting distribution on ϕ is automatically invariant. In other words, for a group element $h \in G$ acting on the space of field configurations \mathbb{R}^{L^2} , given $\rho(hz) = \rho(z)$ and $h(g_\theta(\phi(t), t)) = g_\theta(h\phi(t), t)$ it follows that $p(h\phi(t)) = p(\phi(t))$. In the next section we show how to construct a fully equivariant vector field g_θ .

Method. Inspired by equivariant flows used for molecular modelling [32], we propose to construct a time-dependent vector field for the neural ODE featuring pairwise interactions between the lattice sites and a tensor contraction with a chosen set of basis functions:

$$\frac{d\phi(t)_x}{dt} = \sum_{y,d,f} W_{xydf} K(t) dH(\phi(t)_y)_f. \quad (5)$$

With chosen dimensions D and F , the sums of d and f are taken over $1, \dots, D$ and $1, \dots, F$, respectively. Here, $H : \mathbb{R} \rightarrow \mathbb{R}^F$ is a basis expansion function for the local field values ϕ_y , $K : [0, T] \rightarrow \mathbb{R}^D$ is our chosen time kernel, and $W \in \mathbb{R}^{L^2 \times L^2 \times D \times F}$ is a learnable weight tensor.

Our choice for the basis function is $H(\phi)_1 = \phi$ and $H(\phi)_f = \sin(\omega_f \phi)$ for $f \in \{2, \dots, F\}$, namely a linear term combined with a sine expansion where $\omega \in \mathbb{R}^{F-1}$ are learnable frequencies, inspired by Fourier Features [33]. This choice of basis functions is made in order to respect the global symmetry $\phi \mapsto -\phi$, as is done in [21]. In particular, the cosine function is prohibited by the symmetry. The functional dependence of (5) on ϕ is also chosen so that the divergence of the vector field, necessary for computing the density of the resulting distribution q , can be easily computed analytically.

The time basis functions $K : [0, T] \rightarrow \mathbb{R}^D$ are chosen to be the first D terms of a Fourier expansion on the interval $[0, T]$. This is chosen to allow for simple time-dependent dynamics.

The learnable weight tensor W is initialized to 0, so that the initial flow is the identity map. Linear constraints on the tensor imposed by equivariance with respect to spatial symmetries reduces the number of independent entries of the weight tensor. The spatial symmetry group of the periodic lattice $(\mathbb{Z}/L\mathbb{Z})^{\times 2}$ is $G = C_L^2 \rtimes D_4$, the semi-direct product of two cyclic groups C_L acting as translations, and the Dihedral group D_4 generated by 90-degree planar rotations and the mirror reflection. G -equivariance dictates that W_{xydf} for a given d and f only depends on the orbit of the pair (x, y) . Specifically, for any element g of the symmetry group G acting on a pair of lattice points as $(x, y) \mapsto (gx, gy)$, we have $W_{gx,gy,df} = W_{xydf}$ for all values of x, y, d , and f . Explicitly, since we can use C_L^2 -equivalences to move x to the (arbitrarily chosen) origin given any pair (x, y) , and for most of these pairs there are eight y' satisfying $(x, y) \sim (x, y')$ under D_4 equivalence, the number of free parameters per d and f grows like $L^2/8 + O(L)$ as opposed to L^4 without symmetry constraints.

Finally, we observe that the following factorization of the matrix leads to better training results

$$W_{xydf} = \sum_{d'f'} \tilde{W}_{xyd'f'} W_{d'd}^K W_{f'f}^H \quad (6)$$

with matrices $W^K \in \mathbb{R}^{D' \times D}$, $W^H \in \mathbb{R}^{F' \times F}$. The bond dimensions D' and F' are hyperparameters of the model.

A Theory-Conditional Model. A small change in the parameters of the theory typically leads to a small deformation of its associated distribution, which is reflected in our observation that the network trained for a specific theory still results in a relatively high value of ESS even when applied to a nearby theory with slightly altered parameters. This motivates the extended network architecture and the transfer learning between lattice sizes, as discussed in the current and the following paragraphs respectively.

Instead of a single action S , here we consider a set of theories \mathcal{M} on the lattice. Each theory $\psi \in \mathcal{M}$ is specified by the action $S_\psi : \mathbb{R}^{L^2} \rightarrow \mathbb{R}$, and we can then learn a single neural network to generate samples for all these theories. We do this via an additional basis expansion function $J : \mathcal{M} \rightarrow \mathbb{R}^A$ and a new index to each of the terms in the factorized W tensor: instead of (6), we let

$$W_{xydf}(\psi) = \sum_{d'f'abc} \tilde{W}_{xyd'f'a} J(\psi)_a W_{d'db}^K J(\psi)_b W_{f'fc}^H J(\psi)_c. \quad (7)$$

By choosing a distribution $r(\psi)$ over the theories, the parameters of the model are optimized by maximising the reverse KL divergence averaged over the theories: $\mathbb{E}_{\psi \sim r} \text{KL}(q_\psi | p_\psi)$, where q_ψ is the push-forward distribution using to the map solving the ODE (5) with the conditional weight matrix (7) and p_ψ is the Boltzmann distribution of action S_ψ .

Transfer-Learning Between Lattice Sizes. The parameters W of a model that is trained on a square lattice with L^2 sites may be used as the initial parameters W' for training a model on a larger lattice with length L' . This is an example of transfer learning or curriculum learning [34] and may lead to a speedup compared to training directly on the lattice of length $L' > L$. Roughly speaking, to transfer we embed the kernel W into the kernel W' for the larger lattice. We refer the reader to the appendix

TABLE I: ESS, MCMC acceptance rate and observables ξ and $\chi_2^{(1)}$ for the flow models trained with different lattice sizes L and the corresponding λ tuned to give $L/\xi = 4$ [27].

| L | λ | ESS | MCMC | L/ξ | $\chi_2^{(1)}$ |
|-----|-----------|-----------|-----------|----------|----------------|
| 6 | 6.975 | 99.759(7) | 97.503(4) | 3.968(5) | 1.064(2) |
| 12 | 5.276 | 98.54(2) | 93.367(7) | 3.981(5) | 4.129(6) |
| 20 | 4.807 | 96.63(4) | 89.77(1) | 4.039(5) | 10.59(2) |
| 32 | 4.572 | 91.07(8) | 83.15(2) | 4.031(5) | 25.53(4) |
| 64 | 4.398 | 66(5) | 64.96(2) | 4.012(4) | 91.6(2) |

for details. The frequencies ω_f are kept fixed during the transfer. After initializing the parameters this way, the model can be further trained on the lattice of length L' .

Experiments. For our experiments, we consider the ϕ^4 theory, which has an action as in equation (1) with potential $V(\phi) = \lambda \sum_x \phi_x^4$, specified by the coupling constant λ . In the first experiment, we evaluate the ability of our model as defined in equation (5) to learn to generate samples from a single theory, i.e. for a fixed value of λ . We test this on lattices with length L varying between 6 and 64, where the theory parameter m^2 is held fixed to be $m^2 = -4$, and λ is tuned so that the correlation length ξ approximately equals to 1/4 of the lattice side length. We choose $F = 50$ for the number of field basis functions, $D = 21$ for the number of time kernels, and $F' = 20$, $D' = 20$ for the bond dimensions of the respective factorization matrices. The parameters are optimized by gradient descent, where the expectation in the loss of equation (2) is approximated by averaging over 256 generated samples. More algorithmic details can be found in the appendix.

To assess model quality, we use two different but related metrics, the ESS and the MCMC acceptance rate. We remind the reader that the ESS is a quantity closely related to the acceptance rate. It controls the variance of the mean of N correlated random variables, which scales as $(\text{ESS} \times N)^{-1/2}$. In particular, an ESS of 100% indicates perfectly independent samples and is attained when the target and the proposal distribution coincide. In Figure 1 we report the ESS values against the training time, computed as a moving average over 100 training steps, with the real NVP baseline for comparison, which is based on [18] and was trained for two weeks. For each solid line, the corresponding coupling λ is chosen such that the correlation length is approximately $L/\xi = 4$, as shown in Table I. Our model attains much larger values of the ESS and acceptance rates in much shorter times, for all sizes L , despite the fact that each of its training steps involves integration of an ODE. Table I shows the final ESS and MCMC acceptance rates as well as L/ξ and the two-point susceptibility $\chi_2^{(1)}$ computed with MCMC using the trained flows. Note that the correlation length computed with our flow-assisted MCMC is indeed comparable with that computed using the traditional MCMC method. The description of how ξ , ESS, and two-point susceptibility are estimated is recorded in the appendix. In addition, we demonstrate that transfer learning as described above can be used to reduce the training time for larger lattices. This is shown by dashed lines in Figure 1. All three dashed lines represent a single run of transfer learning between lattice sizes with the target $L = 64$ and the correspondingly fixed value $\lambda = 4.398$. Initially, we train on a theory with $L = 20$ and the λ from Table I listed for $L = 64$. After the ESS approximately saturates during training, the kernel is scaled to size 32×32 and training is continued with the same value of the coupling

constant λ but at $L = 32$. Finally, this is repeated to move to $L = 64$. We observe that, when using transfer learning, it takes a much shorter time to attain a similar value of the ESS when compared to training directly with $L = 64$.

In the final experiment, we train the theory-conditional models as described above and summarized in equation (7) over a range of coupling constants from $\lambda = 4$ to $\lambda = 6$. For the model hyperparameters, we now choose $F = 300$, $F' = 20$ for the field basis functions, $D = 21$, $D' = 20$ for the time kernels, and $A = 50$ for the number of λ basis expansion functions. The latter are chosen to be of the form

$$J(\lambda)_i = \frac{\exp(-w \cdot (\lambda - c_i)^2)}{\sum_j \exp(-w \cdot (\lambda - c_j)^2)}, \quad (8)$$

where w is trainable and the centers c_i are fixed and uniformly spaced in the range of λ . In order to speed up training, we initially train at $L = 12$ and then transfer to $L = 20$ and finally $L = 32$ as described above. For each size, training was continued until the ESS approximately stabilized. Our model achieves high MCMC acceptance rates between 60% and 90% over the whole range of considered theory space. The robustness of the model was tested by performing the training multiple times with different random seeds, which renders similar performance each time as shown in more detail in the appendix.

To demonstrate the physical usefulness of this approach, Figure 3 shows the susceptibility, computed using the estimator $\chi_1^{(2)}$ via MCMC with the trained model as proposal distribution. With the finite-size scaling taken into account, our numerical results display the expected collapse of the curves for different lattice sizes. To obtain these results, a theory conditional flow was trained three times for each lattice size with different random seeds over the range of λ . Using each of the three trained models as proposal, $\chi_1^{(2)}$ was estimated by MCMC. The values shown are the mean while the corresponding standard deviations averaged over λ are 0.3%, 0.5%, 1.6% for $L = 12, 20, 32$, respectively, and are thus too small to be visible in the figure.

Conclusions. In this work we propose a fully equivariant continuous flow model as an effective tool for sampling in lattice field theory. Our experiments indicate that such neurally-augmented sampling is a viable method even for large lattices. Moreover, we have shown that the learned parameters can be meaningfully transferred to nearby theories with different correlation lengths, coupling constants, and lattice sizes, even across the critical point. This makes clear that our approach can be employed for tasks where computations need to be done for families of theories, such as phase transition detection and parameter scans. Finally, we have demonstrated that our flow model can easily incorporate the geometric and global symmetries of the physical system,

resulting in a visible computational advantage which increases with the lattice size. These developments make our flow-model approach a practical tool ready to be employed in lattice field theory computations.

We will end with a comment on a potential interpretation of the learned ODE flow. Note that the flow of the density described by the ODE (4) can readily be interpreted as a flow in the space \mathcal{M} of coupling constants by identifying the probability distribution $p(t)$ as the Boltzmann distribution of a Hamiltonian H_t . As such, it is tantalizing to try to understand the flow in terms of the physical renormalization group of the theory, which also renders a flow in \mathcal{M} . We will report on this in the future.

Acknowledgements. We wish to thank Max Welling for inspiring discussions, Vassilis Anagiannis for his contribution in the early stages of this work, and Jonas Köhler for his helpful suggestions. We also thank Joe Marsh Rossney, Luigi Del Debbio and Uroš Seljak for helpful correspondence.

Appendix

Observables

In the MCMC setting, observables are estimated using a set of N samples $\{\phi^{(i)}\}_{i=1}^N$ from the target distribution. These are generated here by applying the Metropolis-Hasting step on samples proposed by the trained continuous normalizing flows. Here we consider scalar fields on a two-dimensional periodic square lattice of length L , $V_L \cong (\mathbb{Z}/L\mathbb{Z})^2$.

The effective sample size (ESS) is computed as in [18]:

$$\text{ESS} = \frac{\left[\frac{1}{N} \sum_{i=1}^N p(\phi^{(i)})/q(\phi^{(i)}) \right]^2}{\frac{1}{N} \sum_{i=1}^N [p(\phi^{(i)})/q(\phi^{(i)})]^2}. \quad (9)$$

To compute the correlation length ξ we first introduce the estimator for the connected two-point Greens function

$$G(x) = \frac{1}{L^2} \sum_{y \in V_L} \frac{1}{N} \sum_{i=1}^N \left[\phi_y^{(i)} \phi_{x+y}^{(i)} - \phi_y^{(i)} \frac{1}{N} \sum_{j=1}^N \phi_{x+y}^{(j)} \right]. \quad (10)$$

Summing over one of the lattice dimensions, we have

$$G_s(x_2) = \sum_{x_1=1}^L G(x_1, x_2). \quad (11)$$

The correlation length can then be estimated via

$$\frac{1}{\xi} = \frac{1}{L-1} \sum_{x_2=1}^{L-1} \text{arcosh} \left(\frac{G_s(x_2+1) + G_s(x_2-1)}{2G_s(x_2)} \right). \quad (12)$$

The two-point susceptibility is estimated as

$$\chi_2^{(1)} = \sum_{x \in V_L} G(x) = L^2 \left(\frac{1}{N} \sum_{i=1}^N \overline{\phi^{(i)}}^2 - \left(\frac{1}{N} \sum_{i=1}^N \overline{\phi^{(i)}} \right)^2 \right), \quad \text{where} \quad \overline{\phi^{(i)}} = \frac{1}{L^2} \sum_{x \in V_L} \phi_x^{(i)}. \quad (13)$$

In the broken phase, the distribution of $\overline{\phi}$ becomes bimodal. To address this, we introduce an alternative estimator for the two-point susceptibility [35]

$$\chi_2^{(2)} = L^2 \left(\frac{1}{N} \sum_{i=1}^N \overline{\phi^{(i)}}^2 - \left(\frac{1}{N} \sum_{i=1}^N |\overline{\phi^{(i)}}| \right)^2 \right). \quad (14)$$

In the table of estimated observables at different lattice sizes, the ESS was computed 100 times using different random seeds, each time using 500 samples. MCMC of length 10^6 was run 10 times with different random seeds. In both cases, the average and its estimated error are shown. The observables were computed with a single MCMC run of length 10^6 and errors estimated using bootstrap drawing 100 times and with bin size 4. A burn-in phase of length 10^5 was discarded.

Experimental details

Network architecture. The width factor in the chosen form of the λ basis expansion functions $J(\lambda)_i$ should not become negative during training. It is thus parametrized by the trainable parameter \tilde{w} as $w = (A-1) \log(1 + \exp(\tilde{w}))$, which is initialized to $\tilde{w} = \log(e-1)$. The frequencies ω_f are initialised by random uniform values between 0 and 5. Orthogonal initialization was used for the matrices W^K and W^H , while \tilde{W} was initialized with zeros.

Loss computation. The KL-divergence between the network’s output distribution and the theory distribution is computed by a Monte Carlo approximation. For the initial flow model, 256 samples are used in each training step to approximate the integral. To train the theory-conditional flows, a sampling scheme for the considered theory parameters must be chosen. Here, in each training step 8 different values of λ are sampled uniformly in the chosen range. For each, the KL-divergence is computed by a Monte Carlo approximation to the integral with 128 samples. The loss is then the average of the 8 different KL-divergences. The training performance was not observed to strongly depend on the chosen sample sizes. The above values are chosen as a compromise based on available computational resources and are not the result of a comprehensive hyperparameter search.

Optimizer. The flow networks are optimized by minimizing the KL-divergence using stochastic gradient descent. For this, the Adam optimizer is used with a learning rate of 0.005, decaying exponentially by a factor of 0.01 every 8000 steps. After transferring to a larger lattice, the initial learning rate was reduced to 10^{-5} . The decay parameters $\beta_1 = .8$, and $\beta_2 = .9$ of the Adam optimizer were found to improve training speed. The same values were used for all lattice sizes. Training efficiency can likely be improved by tuning these hyperparameters.

Training theory-conditional models. Figure 4 shows the MCMC acceptance rate achieved by training a theory-conditional model over a range of λ couplings from 4 to 6. To demonstrate the robustness of the model, it was independently trained three times with different random seeds. In all runs a similar performance was achieved after training.

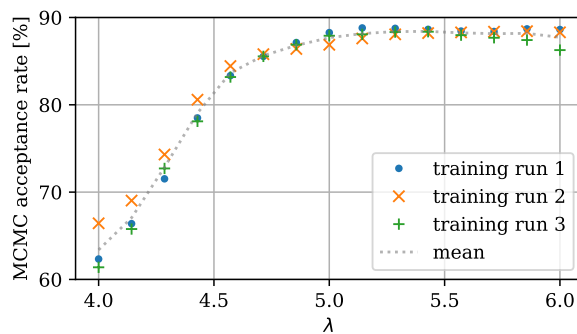


FIG. 4: Acceptance rates of MCMC chains of length 10^6 for a theory-conditional flow trained over a range of λ for $L = 32$.

Symmetries. Figure 5 shows the result of the ablation study we conducted by limiting the symmetries manifestly preserved by the model. We observe a noticeable loss of ESS during training. This becomes more significant as the lattice size is increased. We also observed that models without the full symmetries built-in are more prone to training instabilities when the lattice size increases.

To investigate the effect of having manifest equivariance compared to approximate equivariance learned during training, we look at whether symmetries are broken by the trained real NVP network. The result, shown in Figure 6, shows the quality of the approximation when equivariance of the network is not imposed.

Transfer Learning. To embed the kernel W into the kernel W' for the larger lattice, we consider a pair of points (x, y) in C_L^2 and a pair of points (x', y') in $C_{L'}^2$, and identify $t = y - x \in C_L^2$ with $t = [t_1, t_2]$ with $t_i \in \{-\lfloor \frac{L}{2} \rfloor, \dots, \lfloor \frac{L-1}{2} \rfloor\}$, and similarly $t' = y' - x' = [t'_1, t'_2]$ with $t'_i \in \{-\lfloor \frac{L'}{2} \rfloor, \dots, \lfloor \frac{L'-1}{2} \rfloor\}$. To transfer, we set as initial values $W'_{x'y'af} = W_{xyaf} N_L(t) / N_{L'}(t')$ if $t = t'$, and zero otherwise. The scaling factor $N_L(t) = |\{RtR^{-1} \in C_L^2 \mid R \in D_4\}|$, where RtR^{-1} denotes the action of R on t , is the number of sites reached by rotating/mirroring y around x in a periodic lattice of length L . It accounts for the fact that weights may be used for more pairs in the larger lattice, as illustrated in Figure 7.

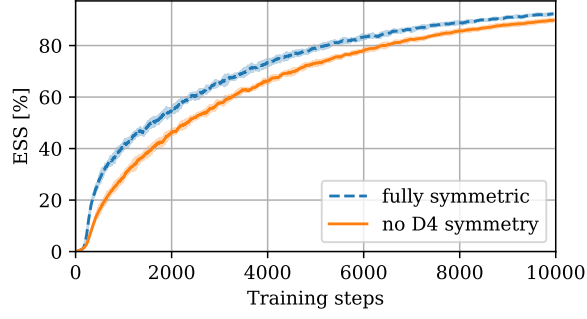


FIG. 5: Training performance of the continuous normalizing flow at $L = 20$ with and without enforcing $D4$ -symmetry. Shown are the mean and standard deviation (shaded area) over 8 training runs with different random seeds, where the shown value of the ESS is the moving average over 100 training steps.

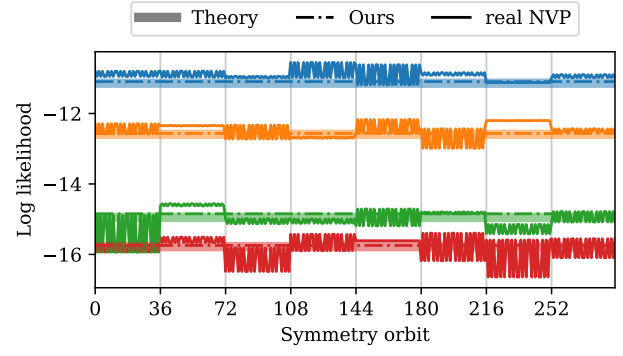


FIG. 6: For 4 samples from an MCMC chain with $L = 6$, we show 1) the true log likelihood given by the action, 2) the model log likelihood of our model and 3) real NVP. Log likelihood of 4 samples of an MCMC chain with $L = 6$. The y -axis shows the likelihoods when the sample is transformed by all 8×6^2 symmetries of the lattice.

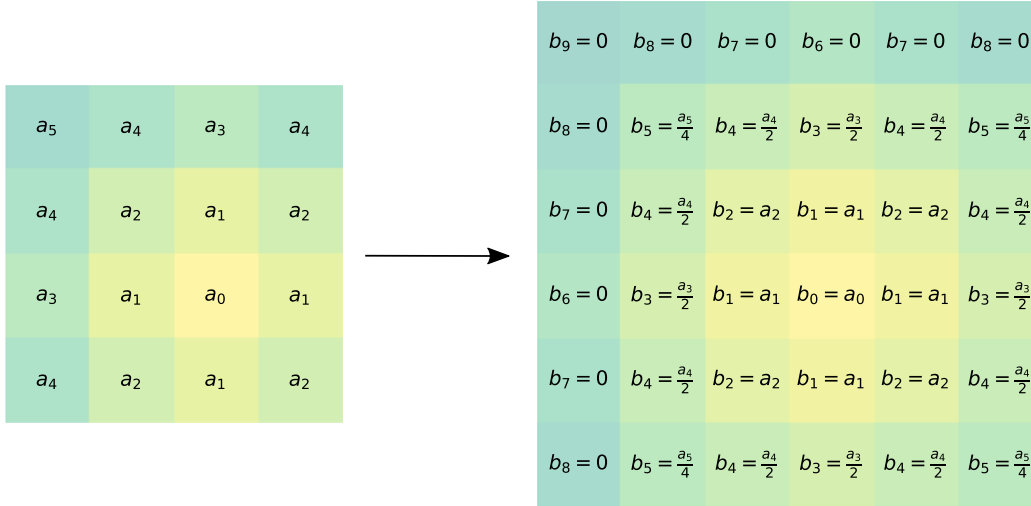


FIG. 7: Illustration of transferring weights W between lattices of size $L = 4$ and $L' = 6$.

-
- [1] K. Binder and D. W. Heermann, *Monte Carlo Simulation in Statistical Physics: An Introduction* (Springer, 2019).
- [2] A. Sokal, Monte carlo methods in statistical mechanics: Foundations and new algorithms, in *Functional Integration: Basics and Applications*, edited by C. DeWitt-Morette, P. Cartier, and A. Folacci (Springer US, Boston, MA, 1997) pp. 131–192.
- [3] A. Tomiya and Y. Nagai, Gauge covariant neural network for 4 dimensional non-abelian gauge theory (2021), arXiv:2103.11965 [hep-lat].
- [4] S. J. Wetzel and M. Scherzer, *Phys. Rev. B* **96**, 184410 (2017).
- [5] S. Blücher, L. Kades, J. M. Pawłowski, N. Strodthoff, and J. M. Urban, *Phys. Rev. D* **101**, 094507 (2020).
- [6] D. L. Boyda, M. N. Chernodub, N. V. Gerasimeniuk, V. A. Goy, S. D. Liubimov, and A. V. Molochkov, *Phys. Rev. D* **103**, 014509 (2021).
- [7] B. Yoon, T. Bhattacharya, and R. Gupta, *Phys. Rev. D* **100**, 014504 (2019).
- [8] R. Zhang, Z. Fan, R. Li, H.-W. Lin, and B. Yoon, *Phys. Rev. D* **101**, 034516 (2020).
- [9] T. Matsumoto, M. Kitazawa, and Y. Kohno, *Progress of Theoretical and Experimental Physics* **2021**, 10.1093/ptep/ptaa138 (2020), 023D01.
- [10] A. Tanaka and A. Tomiya, Towards reduction of autocorrelation in hmc by machine learning (2017).
- [11] K. Zhou, G. Endrődi, L.-G. Pang, and H. Stöcker, *Phys. Rev. D* **100**, 011501 (2019).
- [12] J. M. Pawłowski and J. M. Urban, *Mach. Learn. Sci. Tech.* **1**, 045011 (2020), arXiv:1811.03533 [hep-lat].
- [13] Y. Nagai, A. Tanaka, and A. Tomiya, Self-learning monte-carlo for non-abelian gauge theory with dynamical fermions (2020).
- [14] M. Albergò, G. Kanwar, and P. Shanahan, *Physical Review D* **100**, 034515 (2019).
- [15] D. J. Rezende, G. Papamakarios, S. Racaniere, M. Albergò, G. Kanwar, P. Shanahan, and K. Cranmer, in *Proceedings of the 37th International Conference on Machine Learning*, Proceedings of Machine Learning Research, Vol. 119, edited by H. D. III and A. Singh (PMLR, 2020) pp. 8083–8092.
- [16] G. Kanwar, M. S. Albergò, D. Boyda, K. Cranmer, D. C. Hackett, S. Racanière, D. J. Rezende, and P. E. Shanahan, *Phys. Rev. Lett.* **125**, 121601 (2020).
- [17] D. Boyda, G. Kanwar, S. Racanière, D. J. Rezende, M. S. Albergò, K. Cranmer, D. C. Hackett, and P. E. Shanahan, *Phys. Rev. D* **103**, 074504 (2021).
- [18] M. S. Albergò, D. Boyda, D. C. Hackett, G. Kanwar, K. Cranmer, S. Racanière, D. J. Rezende, and P. E. Shanahan, Introduction to normalizing flows for lattice field theory (2021), arXiv:2101.08176 [hep-lat].
- [19] L. Vaitl, K. A. Nicoli, S. Nakajima, and P. Kessel, in *International Conference on Machine Learning* (PMLR, 2022) pp. 21945–21959.
- [20] R. Abbott, M. S. Albergò, A. Botev, D. Boyda, K. Cranmer, D. C. Hackett, G. Kanwar, A. G. D. G. Matthews, S. Racanière, A. Razavi, D. J. Rezende, F. Romero-López, P. E. Shanahan, and J. M. Urban, Sampling qcd field configurations with gauge-equivariant flow models (2022).
- [21] K. A. Nicoli, C. J. Anders, L. Funcke, T. Hartung, K. Jansen, P. Kessel, S. Nakajima, and P. Stornati, *Phys. Rev. Lett.* **126**, 032001 (2021), arXiv:2007.07115 [hep-lat].
- [22] K. A. Nicoli, S. Nakajima, N. Strodthoff, W. Samek, K.-R. Müller, and P. Kessel, *Phys. Rev. E* **101**, 023304 (2020), arXiv:1910.13496 [cond-mat.stat-mech].
- [23] L. Dinh, J. Sohl-Dickstein, and S. Bengio, Density estimation using real nvp (2017), arXiv:1605.08803 [cs.LG].
- [24] K. A. Nicoli, C. Anders, L. Funcke, T. Hartung, K. Jansen, P. Kessel, S. Nakajima, and P. Stornati, arXiv preprint arXiv:2111.11303 (2021).
- [25] L. Del Debbio, J. M. Rossney, and M. Wilson, *Phys. Rev. D* **104**, 094507 (2021), arXiv:2105.12481 [hep-lat].
- [26] D. C. Hackett, C.-C. Hsieh, M. S. Albergò, D. Boyda, J.-W. Chen, K.-F. Chen, K. Cranmer, G. Kanwar, and P. E. Shanahan, Flow-based sampling for multimodal distributions in lattice field theory (2021), arXiv:2107.00734 [hep-lat].
- [27] I. Vierhaus, *Simulation of φ^4 theory in the strong coupling expansion beyond the Ising limit*, Ph.D. thesis, Humboldt University (2010).
- [28] G. Mussardo, *Statistical Field Theory: An Introduction to Exactly Solved Models in Statistical Physics*, Oxford Graduate Texts (OUP Oxford, 2010).
- [29] I. Montvay and G. Münster, *Quantum fields on a lattice* (Cambridge University Press, 1997).
- [30] F. Noé, S. Olsson, J. Köhler, and H. Wu, *Science* **365** (2019).
- [31] T. Q. Chen, Y. Rubanova, J. Bettencourt, and D. K. Duvenaud, in *Advances in neural information processing systems* (2018) pp. 6571–6583.
- [32] J. Köhler, L. Klein, and F. Noe, in *Proceedings of the 37th International Conference on Machine Learning*, Proceedings of Machine Learning Research, Vol. 119, edited by H. D. III and A. Singh (PMLR, 2020) pp. 5361–5370.
- [33] M. Tancik, P. P. Srinivasan, B. Mildenhall, S. Fridovich-Keil, N. Raghavan, U. Singhal, R. Ramamoorthi, J. T. Barron, and R. Ng, arXiv preprint arXiv:2006.10739 (2020).
- [34] Y. Bengio, J. Louradour, R. Collobert, and J. Weston, in *Proceedings of the 26th annual international conference on machine learning* (2009) pp. 41–48.
- [35] A. W. Sandvik, *AIP Conference Proceedings* **1297**, 135 (2010).